

# SDFit: 3D Object Pose and Shape by Fitting a Morphable SDF to a Single Image

Dimitrije Antić<sup>1</sup> Sai Kumar Dwivedi<sup>2</sup> Shashank Tripathi<sup>2</sup> Theo Gevers<sup>1</sup> Dimitrios Tzionas<sup>1</sup>

<sup>1</sup>University of Amsterdam, The Netherlands <sup>2</sup>Max Planck Institute for Intelligent Systems, Tübingen, Germany

{d.antic, th.gevers, d.tzionas}@uva.nl {sdwivedi, stripathi}@tue.mpg.de

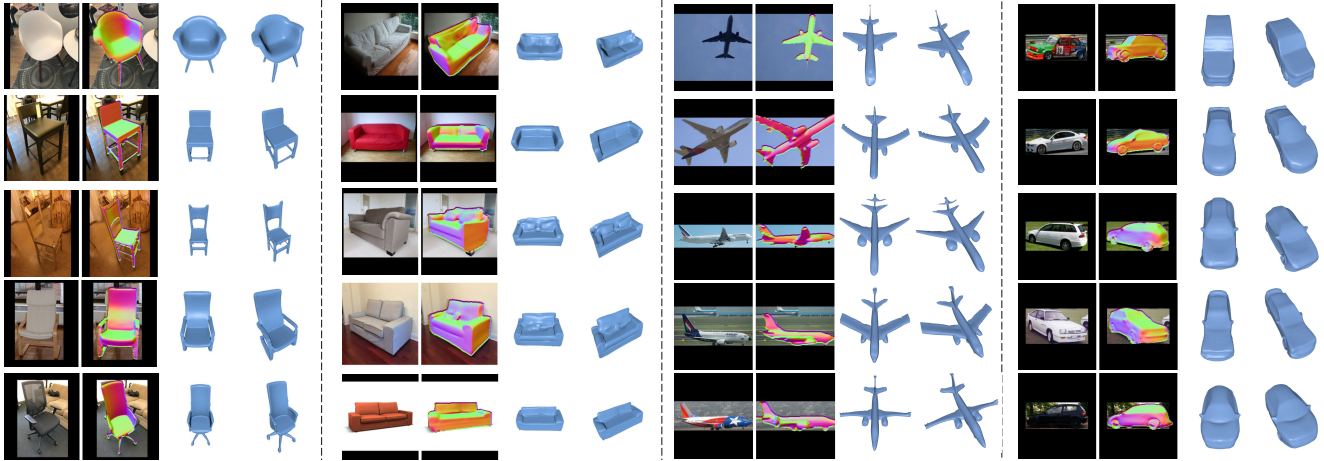


Figure 1. We present SDFit, a novel framework that recovers an object’s 3D shape and pose from a single image. To this end, SDFit uses a learned, category-level, morphable SDF (mSDF) shape model, and specifically DIT [75], and fits this to images in a render-and-compare fashion by computing rich 2D-to-3D correspondences via recent foundational models. SDFit shows promising results and scalability while requiring no-retraining for in-the-wild images. For overlays we show mSDF normals for visualization reasons. **Q Zoom in** to see details.

## Abstract

We focus on recovering 3D object pose and shape from single images. This is highly challenging due to strong (self-)occlusions, depth ambiguities, the enormous shape variance, and lack of 3D ground truth for natural images. Recent work relies mostly on learning from finite datasets, so it struggles generalizing, while it focuses mostly on the shape itself, largely ignoring the alignment with pixels. Moreover, it performs feed-forward inference, so it cannot refine estimates. We tackle these limitations with a novel framework, called SDFit. To this end, we make three key observations: (1) Learned signed-distance-function (SDF) models act as a strong morphable shape prior. (2) Foundational models embed 2D images and 3D shapes in a joint space, and (3) also infer rich features from images. SDFit exploits these as follows. First, it uses a category-level morphable SDF (mSDF) model, called DIT, to generate 3D shape hypotheses. This mSDF is initialized by querying OpenShape’s latent space conditioned on the input image. Then, it computes 2D-to-3D correspondences, by extracting and matching features from the image and mSDF. Last, it

fits the mSDF to the image in an render-and-compare fashion, to iteratively refine estimates. We evaluate SDFit on the Pix3D and Pascal3D+ datasets of real-world images. SDFit performs roughly on par with state-of-the-art learned methods, but, uniquely, requires no re-training. Thus, SDFit is promising for generalizing in the wild, paving the way for future research. Code will be released.

## 1. Introduction

Recovering 3D object pose and shape (OPS) from single color image is key for building intelligent systems and mixed realities. The task is highly ill-posed due to strong challenges such as depth ambiguities, (self-)occlusions, and the huge variance in shape, appearance, and viewpoint. Yet, humans routinely solve this task; we effortlessly navigate rooms, detect objects, and infer their layout, by building and exploiting rich prior models through experience. Despite progress, computers still lack reliable methods and priors for reconstructing 3D objects from natural images. Our goal is to recover both 3D object shape and pose, jointly.

To this end, we draw inspiration from the “analogous” task of human pose and shape (HPS) estimation. HPS is nowadays relatively reliable, largely thanks to morphable generative body models [2, 30, 53, 70], such as SMPL [42]. These are data-driven and capture shape variance across a database of 3D body scans. When fitting these models to a single image [53, 67, 70], such as with the SMPLify [6] method, they act as a strong prior; e.g., full body shape can be inferred from a partial body view with cropped legs. Such fitting also facilitates deep learning, as training HPS regressors partially requires 3D pseudo-GT datasets [6, 13, 31, 37] collected by fitting SMPL to 2D keypoints detected in unlabeled images [7].

It is probably fair to say that monocular HPS methods are more reliable than OPS ones. Note that no SMPL-like model or SMPLify-like method exists so far for objects. The question arises: “Can we solve OPS by trivially adapting HPS methods for this?” The answer is a “no” as, despite commonalities, these tasks differ in three key factors: (1) Shape variance is much higher for objects (both intra- and inter-class) than for bodies (only intra-class). For example, an armchair looks different from an airplane, but also from an office chair, rocking chair, or folding chair. (2) Bodies have the same topology, while object topology varies wildly (e.g., chairs have a varying number of legs). (3) To guide HPS fitting, OpenPose-like methods [7, 43] robustly detect 2D joints in images, corresponding to 3D SMPL joints. In contrast, for general objects, detecting keypoints in 2D images and correspondences with a morphable 3D model is largely unsolved. Consequently, OPS and HPS methods have evolved separately.

The current OPS paradigm is rendering synthetic images using 3D databases [15, 16, 66] and training deep networks on these for regressing 3D shape from an image [1, 25–27], or generating it with diffusion conditioned on the image [12, 17, 32, 45, 46, 49]. These are promising, but have three limitations: (1) They struggle generalizing to real images. (2) Most methods perform only feed-forward inference, so they lack a feedback loop for refining erroneous estimates. (3) They mostly focus on geometry alone, largely ignoring object or camera pose, and by extension, pixel alignment.

We tackle these with a novel framework, called SDFit; a high-level overview is shown in Fig. 2. At the core lies a category-level morphable signed-distance function (mSDF) that generates 3D shape hypotheses (analogous to SMPL [42]); here we use DIT [75]. The mSDF lies on the manifold of valid shapes while allowing for arbitrary topologies [52, 61, 75]. Moreover, it has a compact latent space, so it facilitates fitting by constraining the search space. It also establishes dense correspondences across morphed shapes. Our SDFit framework fits this mSDF to an image by optimizing the latent code (shape) and pose, in a render-and-compare fashion (analogous to SMPLify [6]).

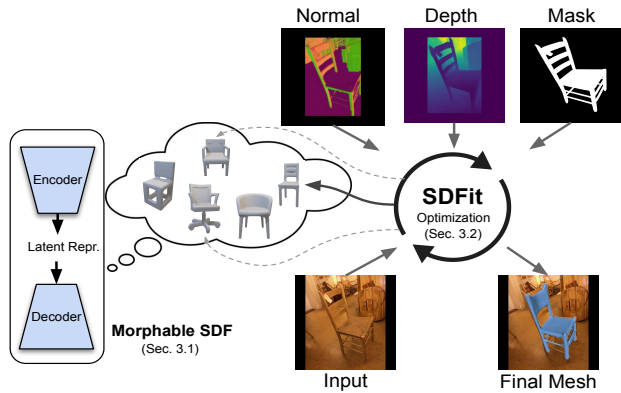


Figure 2. High-level overview of our SDFit framework. To recover 3D object pose and shape, we fit a morphable signed-distance function (mSDF) model to observed image features (i.e., extracted normal, depth and binary masks) in a render-and-compare fashion. This results in a pixel-aligned 3D shape reconstruction.

This is far from trivial, as it requires a good initialization for both 3D shape and pose. However, these problems are largely unsolved for everyday objects (in contrast to HPS); thus, we need the following methodological advancements.

**Shape initialization:** Foundational models [24, 38, 76] can nowadays embed many modalities into a joint latent space. We exploit this for a novel shape retrieval. First, offline, we embed ShapeNet [8] meshes (and by extension respective mSDF codes) into OpenShape’s [38] latent space. Online, we embed an image into the same latent space, and find the nearest-neighbor mSDF shape. This is simple, yet effective.

**Pose initialization:** Foundational models also extract rich features. First, we extract rich features [50, 59, 74] from the input image. Then, offline, we “decorate” [72] our 3D mSDF with such features, by rendering multi-view images of its template, computing features for these images, and back-projecting these onto the 3D template. Crucially, online, the “decorated” features “follow” the mSDF as this morphs, via its inherent shape correspondences. In this way, we establish 2D-to-3D (image-to-mSDF) correspondences, which help us solve for 3D pose through RANSAC and PnP.

**Fitting:** After initialization, we refine 3D shape and pose via render-and-compare fitting. That is, we estimate feature maps from the image (mask, depth, and normal maps), render such maps for the running mSDF hypothesis, and iteratively minimize the discrepancy of these until convergence.

We quantitatively evaluate SDFit on two tasks: (1) 3D shape estimation, and (2) image alignment (involving both 3D shape and pose estimation). We use two in-the-wild datasets, i.e., Pix3D [62] and Pascal3D+ [68]. Our fitting-based SDFit framework performs roughly on par with modern learned models, both regression- [27] and diffusion-based [12] ones. However, SDFit shows a unique promise for generalizing in the wild, as it requires no re-training for unseen natural images. Moreover, it inherently tackles both shape and pose as first-class citizens during inference.

In summary, the main contributions of our work here are: (1) A novel optimization-based framework, called SDFit, that uses a 3D morphable SDF (mSDF) model as a strong (implicit) shape prior, and fits this to single color images. (2) A novel mSDF shape initialization, casted as a retrieval problem in a joint latent space of 2D images and 3D shapes. (3) A novel mSDF pose initialization, using foundational models to establish rich image-to-mSDF correspondences.

We believe that SDFit is a promising direction that opens up ways for future research. Source code will be released.

## 2. Related Work

Here we discuss work on 3D shape inference, joint pose and shape inference, as well as 3D-aware foundational models.

**Object Shape Estimation:** Recent work in 3D shape inference from images represents shape in two key ways: (1) explicit representations like voxel grids [11, 14], point clouds [19, 65], polygonal meshes [1, 21, 26, 64] and (2) implicit representations such as Neural Radiance Fields (NeRF) [28, 55] or Signed-Distance Fields (SDF) [52, 75]. The former is easier to model but struggles with complex structures, while the latter provides more compact and flexible alternatives by encoding shapes as continuous fields. We follow the latter, and specifically SDFs.

Approaches for 3D shape estimation follow three main paradigms, namely they are based on regression [1, 25–27, 71], generative [12, 32, 40, 45, 49] and retrieval [38, 76].

Regression methods have significantly advanced 3D shape reconstruction from single images. This includes methods like SS3D [1], which is pretrained on ShapeNet [8] and fine-tuned on real-world images, while category-specific models are constructed to improve performance. ShapeClipper [26] further enhances this with CLIP-based shape consistency. Similarly, LRM [25] predicts NeRF using a transformer, achieving detailed 3D reconstruction. Recently, ZeroShape [27] infers camera intrinsics and depth as proxy states to improve reconstruction. However, these models often struggle generalizing to unseen categories and capturing the full diversity of complex or real-world shapes.

Generative methods, like Zero123 [40], leverage foundational models for 3D shape estimation utilizing diffusion models to generate novel views from a single image, which are then used in multiview-to-3D methods such as One-2-3-45 [39, 56]. However, appearance quality (which is usually the priority) trades off against geometry quality. SDFusion [12] learns an image-conditioned diffusion process on the latent representation of object SDF.

Retrieval methods such as OpenShape [38] align multi-modal data, such as images and point clouds. Then, given an image, they retrieve the closest-looking 3D object from a database. However, 3D databases have finite sizes, thus, retrieved shapes might not accurately match input images.

**Object Pose and Shape Estimation:** Recent single-image object pose estimation falls into two main categories: (1) direct pose parameter estimation [21, 69] and (2) alignment of a 3D template model with an input modality (e.g., image, feature, keypoints) [10, 22, 41, 63]. The first approach directly predicts rotation, translation, and scale using neural networks. The second approach predicts either sparse correspondences [22, 41], dense 3D-3D correspondences [63], or dense 3D-2D ones [10, 51]. After establishing 3D template correspondences, these methods use PnP optimization [9] to determine the pose. While effective, they depend on inputs like accurate camera or depth data and struggle generalizing to unseen objects. Importantly, they also require an a-priori known shape.

More recently, ROCA [23] jointly estimates object pose and shape. To this end, it applies differentiable Procrustes optimization on a retrieved CAD model, improving pose estimation. However, the fixed shape of CAD models compromises reconstruction. Similarly, Pavllo et al. [55] also estimate pose and shape using NeRF, without refinement.

In contrast, SDFit optimizes both pose and shape using 3D-aware feature “decoration” through foundation models.

**3D-aware Foundational Models:** Large foundational models have catalyzed many 2D vision tasks [4]. Banani et al. [5] find that DINOv2 [50] and StableDiffusion [59] features also facilitate 3D tasks. We use features from these models to establish dense image-to-3D correspondences.

## 3. Method

We recover 3D object pose and shape (OPS) from a single image through a novel render-and-compare framework, called SDFit. At the core of this lies a category-level 3D morphable signed-distance function (mSDF) (Sec. 3.1), and exploiting recent foundational models [38, 50, 59, 74].

Our SDFit framework fits the mSDF to image cues (Sec. 3.2) by jointly optimizing over its shape and pose. However, optimization-based methods are prone to local minima, so they need a good initialization. To this end, SDFit first initializes the mSDF shape through a state-of-the-art (SotA) retrieval-based technique (Sec. 3.3). Then, it initializes pose by aligning the initial shape to rich foundational features extracted from the image (Sec. 3.4).

### 3.1. Shape Representation

We represent 3D object shape via a category-level learned morphable signed-distance function (mSDF).

**mSDF:** Here we use the pretrained DIT model [75]. Each shape is encoded by a unique latent code,  $\mathbf{z} \in \mathbb{R}^{256}$ , in a compact space learned by auto-decoding a 3D dataset [8]. Mapping any 3D point,  $x$ , to a signed distance is parameterized by a network  $f_{\theta}^{sdf} : \mathbb{R}^{3 \times 256} \rightarrow \mathbb{R}$  (with weights  $\theta$ ) conditioned on latent  $\mathbf{z}$ . Each 3D shape,  $S$ , is encoded as the mSDF’s 0-level set,  $S = \{x \in \mathbb{R}^3 \mid f_{\theta}^{sdf}(x; \mathbf{z}) = 0\}$ .

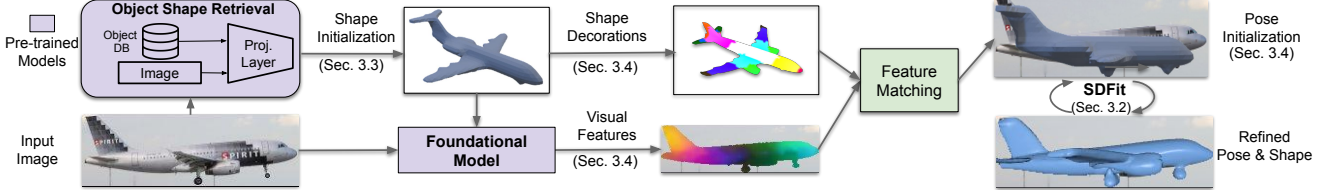


Figure 3. Our SDFit framework. We represent 3D shape via a learned morphable signed-distance function (mSDF) model [75] (Sec. 3.1). We first recover a likely initial shape from a database [8] via a SotA retrieval method [38] conditioned on the input image (Sec. 3.3). Next, we extract features from both the target image and the initial shape via foundational models [50, 74] to establish image-to-mSDF correspondences and initialize pose (Sec. 3.4). Finally, we iteratively refine both shape and pose in a render-and-compare fashion (Sec. 3.2).

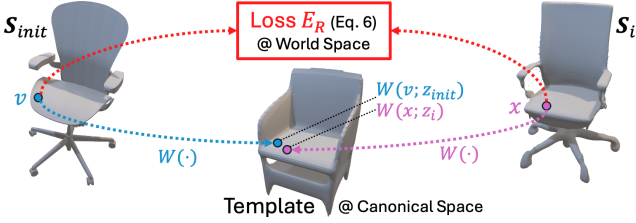


Figure 4. Loss  $E_R$  (Eq. (6)). Initial and hypothesis shapes,  $S_{init}$  and  $S_i$ , are warped to a canonical space via DIT’s warper  $W(\cdot)$ . For each warped vertex of  $S_i$  we find the closest warped vertex of  $S_{init}$  in canonical space, and compute MSE in world space.

DIT decodes a latent  $\mathbf{z}$  into signed distances through a warping function,  $W(x; \mathbf{z})$ , that “warps” any 3D point,  $x$ , to a canonical space defined by a learned category-level SDF template,  $T$ . This models the inter-category shape variance w.r.t. the template, and defines dense correspondences to it.

Note that training DIT on ShapeNet [8] shapes comes with a useful byproduct, that is, it yields a collection of latent codes,  $\mathcal{Z}$ , for these shapes, where  $\mathbf{z} \in \mathcal{Z}$ . We use these later to initialize our shape hypothesis (Sec. 3.3) for fitting.

**Rendering:** Rendering an mSDF is not straightforward, so we extract a 3D mesh as a proxy for differentiable rendering. In the following,  $f_\theta^{shape}(\mathbf{z}; \mathbf{X}, R, t)$  refers to a composite function of three steps: (1) predicting SDF values via  $f_\theta^{sdf}$  on a 3D grid,  $\mathbf{X} \in \mathbb{R}^{N \times N \times N}$ , (2) extracting a mesh using FlexiCubes [60]; and (3) posing it by applying a 6-DoF rigid transformation  $(R, t) \in \text{SE}(3)$ .

### 3.2. Fitting Pose & Shape

To recover OPS from an image, we optimize over object shape,  $\mathbf{z} \in \mathbb{R}^{256}$ , scale,  $\mathbf{s} \in \mathbb{R}^3$ , and pose,  $(R, t) \in \text{SE}(3)$ , by minimizing the energy function via render-and-compare:

$$E = E_{\mathcal{M}} + \lambda_{\mathcal{N}} E_{\mathcal{N}} + \lambda_{\mathcal{D}} E_{\mathcal{D}} + \lambda_{DT} E_{DT} + \lambda_R E_R, \quad (1)$$

where  $\mathcal{M}$  is the mask,  $\mathcal{N}$  the normal map,  $\mathcal{D}$  the depth map, DT denotes a 2D distance transform, R denotes regularization, and  $\lambda$  are steering weights.

The individual energy terms are:

$$E_{\mathcal{M}} = \text{MSE}(\widehat{\mathcal{M}}^i, \mathcal{M}) + \lambda_{IoU} \cdot \text{IoU}(\widehat{\mathcal{M}}^i, \mathcal{M}), \quad (2)$$

$$E_{\mathcal{D}} = \text{SSI-MAE}(\widehat{\mathcal{D}}^i, \mathcal{D}), \quad (3)$$

$$E_{\mathcal{N}} = \text{MSE}(\widehat{\mathcal{N}}^i, \mathcal{N}), \quad (4)$$

$$E_{DT} = \sum_{x \in \widehat{\mathcal{C}}^i} \min_{\tilde{x} \in \mathcal{C}} \|x - \tilde{x}\|_1. \quad (5)$$

where non-hat symbols are “ground-truth” observations, hat denotes maps rendered from the running mSDF hypothesis,  $i$  is the running iteration,  $\mathcal{C}$  the mask contour,  $\text{MSE}$  the mean squared error,  $\text{IoU}$  the intersection-over-union, while SSI-MAE is a scale- and shift-invariant depth loss [57].

To regularize fitting under self-occlusions (Sec. 3.1) a regularization loss,  $E_R$ , encourages the running shape hypothesis,  $S_i$ , to be consistent with the initial estimate,  $S_{init}$  (Sec. 3.3). A simple way would be to penalize deviation of the running  $\mathbf{z}$  latent code from the code  $\mathbf{z}_{init}$  of  $S_{init}$ , but this causes strong local minima when  $S_{init}$  has a wrong topology (e.g. a chair that erroneously misses armrests).

Instead, we geometrically regularize to  $S_{init}$  so we can still refine topology (e.g. chairs growing missing armrests). To this end, we use the correspondences of  $S$  and  $S_{init}$  to the template,  $T$ , to map each vertex  $x \in S_i$  to the closest vertex  $u \in S_{init}$ . More specifically, as shown in Fig. 4, (1) we warp  $S_i$  vertices on the template in *canonical space*, (2) we warp  $S_{init}$  vertices on the same template as well, and (3) for each warped vertex of  $S_i$  we find the closest warped vertex of  $S_{init}$ , and eventually (4) we compute the MSE for corresponding vertices in *world space*. In technical terms:

$$E_R = \text{MSE}(S_i, S_{init}), \quad (6)$$

$$S_{init} = \{v \mid \arg \min_{v \in S_{init}} \|W(v; \mathbf{z}_{init}) - W(x; \mathbf{z}_i)\|_2\}, \quad (7)$$

where  $x \in S_i$  are vertices of  $S_i$ ,  $W(x; \mathbf{z}_i)$  are these vertices mapped into the canonical space via the warper  $W(\cdot)$ ,  $v \in S_i$  are vertices of  $S_{init}$ ,  $W(v; \mathbf{z}_{init})$  are these vertices mapped into the canonical space, and  $S_i = f_\theta^{shape}(\mathbf{z}_i; \mathbf{X})$  is the  $i$ -th iteration shape hypothesis (in canonical space).

During optimization, in each iteration, we evaluate the energy function  $E$  of Eq. (1), backpropagate the gradients, and update our hypothesis parameters  $\mathbf{z}_i$ ,  $R_i$ , and  $t_i$ .

### 3.3. Shape Initialization

Optimization-based frameworks need a good initialization, let alone for single-view inputs. To this end, we initialize the shape code  $\mathbf{z}$  by exploiting the retrieval-based OpenShape [38] model, denoted as  $f^{db}$ . This encodes multiple modalities (text, images, 3D point clouds) into a joint latent space, and facilitates searching for the 3D object,  $S_{init}$ , that looks closer to an input image,  $\mathcal{I}$ , via three steps: (1) we encode each shape in the mesh database  $\mathcal{S}$  via  $f^{db}$ ; (2) we embed an image into the same latent space via  $f^{db}$ ; (3) we retrieve the shape whose embedding (latent code  $\mathbf{z}$ ) most closely lies to the image embedding. More formally, the initial-shape latent code,  $\mathbf{z}_{init}$ , is the code  $\mathbf{z}$  whose 3D shape embedding,  $f^{db}(f_{\theta}^{shape}(\mathbf{z}; \mathbf{X}))$  lies closest to the input-image embedding,  $f^{db}(\mathcal{I})$ , via the similarity metric:

$$\mathbf{z}_{init} = \arg \max_{\mathbf{z} \in \mathcal{Z}} \frac{f^{db}(\mathcal{I}) \cdot f^{db}(f_{\theta}^{shape}(\mathbf{z}; \mathbf{X}))}{\|f^{db}(\mathcal{I})\|_2 \|f^{db}(f_{\theta}^{shape}(\mathbf{z}; \mathbf{X}))\|_2}, \quad (8)$$

where  $\mathbf{X} \in \mathbb{R}^{N \times N \times N}$  is a 3D grid,  $\mathbf{z}$  is the shape latent code, and  $\mathcal{Z}$  is a database of auto-decoded latent codes, each corresponding to a shape instance in the mSDF training set.

### 3.4. Pose Initialization

Apart from initializing object shape (Sec. 3.3) we also need to initialize object pose, to align object geometry to image pixels. But estimating 3D pose from a single view is highly ill-posed. To tackle this: (1) we establish correspondences between 2D pixels and 3D points, (2) estimate camera intrinsics, (3) filter out noisy correspondences with RANSAC, and (4) apply the Perspective-n-Point (PnP) method.

To find correspondences we compute image features from the input image and rendered mSDF images. To this end, inspired from image-to-image matching, we leverage features from foundational models such as StableDiffusion (SD) [59] (or ControlNet [74]) and DINOv2 [50]. Specifically, we compute hybrid features that combine SD v1.5 (ControlNet) and DINOv2 ones, as these encode geometry and semantic cues [18, 44, 72] that are crucial for 3D understanding. In detail, we establish 2D-to-3D pixel-vertex correspondences as described in the following paragraphs.

**Image Features:** We use the pretrained ControlNet [74] and DINOv2 [50] models. We condition ControlNet on the prompt ``A <category>, photorealistic, real-world`` and on normal and depth maps estimated from an image, for inpainting [18], i.e., hallucinating the original image from condition signals. Crucially, this pushes ControlNet to semantically differentiate between nearby pixels [18], so features extracted from its layers capture *semantic* cues. Then, we apply DINOv2 [50] on an image to extract features capturing *geometric* cues [5]. Last, we form hybrid features by per-pixel concatenating the complementary ControlNet and DINOv2 features.



Figure 5. Features for mSDF. Instead of decorating from scratch every morphed mSDF shape, we query pre-computed features via DIT’s correspondences (shown colorcoded) and warper,  $W(\cdot)$ . We either pre-decorate the template  $T$  once per category ( $\text{feat}@T$ ), or the initial shape  $S_{init}$  once per image ( $\text{feat}@S_{init}$ ).

In technical terms, for an input image  $\mathcal{I}$ , estimated normal and depth maps,  $\mathcal{N}$  and  $\mathcal{D}$ , and a text prompt, we use a pretrained ControlNet to generate (inpaint) a “textured” image  $\mathcal{I}^{tex}$ . To get ControlNet features, at the last diffusion step we extract features  $\mathcal{F}_2^{diff}$  and  $\mathcal{F}_4^{diff}$  from its UNet decoder layers 2 and 4, respectively, upsample these to the resolution of  $\mathcal{I}$ , and concatenate these to obtain the feature  $\mathcal{F}^{diff} = \{\mathcal{F}_2^{diff} \parallel \mathcal{F}_4^{diff}\}$ . Note that here features from early layers emphasize semantic and geometric cues over texture ones [5, 18], which suits us. To get  $\mathcal{F}^{DINOv2}$  features, we apply the DINOv2 model on the textured image  $\mathcal{I}^{tex}$  (applicable also for the mSDF, see next paragraph), to extract per-pixel geometric cues. To form the final features we concatenate [72] per pixel the normalized  $\mathcal{F}^{diff}$  features with  $\mathcal{F}^{DINOv2}$  ones, as  $\mathcal{F} = \{\alpha \mathcal{F}^{diff}, (1 - \alpha) \mathcal{F}^{DINOv2}\}$ , where  $\alpha$  is a steering weight.

We focus only on object pixels via a detection mask,  $\mathcal{M}$ . For simplicity, we denote the flattened feature  $\mathcal{F}_{M(\mathcal{I})}$  as  $\mathcal{F}_{\mathcal{I}}$ .

**Shape (mSDF) Features:** Recently, Diff3F [18] introduces a method for decorating 3D meshes with features extracted via the ControlNet and DINO foundational models. We follow this to obtain features for the mSDF, and exploit these for zero-shot correspondence matching with image features. Note that our mSDF model of choice, i.e., DIT [75], establishes dense correspondences across all morphed shapes within a category. Crucially, this means that we don’t have to re-decorate the mSDF due to morphing at every fitting step. Instead, we decorate a mesh extracted from the mSDF only once (details below), and for every morphed shape we “query” features from it via the correspondences.

The above can be performed in two different ways: (1) “SDFit feat@T” (Fig. 5-left): We decorate a mesh extracted from the mSDF template,  $T$ . We do this offline, once per category. Then, for every morphed mSDF shape, we query decoration features from the already decorated  $T$ . (2) “SDFit feat@S<sub>init</sub>” (Fig. 5-right): We decorate a mesh extracted from the initial mSDF shape,  $S_{init}$  (Sec. 3.3). We run this once per image, as  $S_{init}$  differs across images. During morphing, we query features from the decorated  $S_{init}$ . These options trade efficiency for accuracy; the former is computationally cheaper, but the latter is more accurate.

In any case, for decoration we first extract a mesh [60] from either  $T$  or from  $S_{init}$ . Then, we sample  $J$  views on a unit sphere around it, and for each view  $j \in J$ , we render normal maps,  $\hat{\mathcal{N}}^j$ , and depth maps,  $\hat{\mathcal{D}}^j$ . Then, we extract per-pixel feature maps,  $\mathcal{F}_{\mathcal{I}}^j$ , in the same way as for image features, discussed above. Since we know the camera parameters,  $P^j$ , we unproject each view-specific feature map,  $\mathcal{F}_{\mathcal{I}}^j$ , onto 3D mesh vertices. Last, for each vertex we aggregate the unprojected features across views, and obtain the final feature,  $\mathcal{F}_S \in \mathbb{R}^{|S| \times 2368}$ , where  $|S|$  is the number of vertices and 2368 is the feature dimension.

**Object-to-Image Alignment:** Using the extracted image and shape feature maps,  $\mathcal{F}_{\mathcal{I}}$  and  $\mathcal{F}_S$ , respectively, we compute the cosine similarity matrix:

$$\mathcal{A}_{i,s} = \frac{\mathcal{F}_{\mathcal{I}}^i \cdot \mathcal{F}_S^s}{\|\mathcal{F}_{\mathcal{I}}^i\|_2 \|\mathcal{F}_S^s\|_2}, \quad (9)$$

where  $\mathcal{F}_{\mathcal{I}}^i$  and  $\mathcal{F}_S^s$  are  $i$ -th pixel and  $s$ -th vertex features. We then establish pixel-vertex correspondences,  $\mathcal{C}$ , by finding in feature space the most similar vertex for each pixel:

$$\mathcal{C} = \{\{i, s\} = \arg \max_{s \in S_{init}} \mathcal{A}_{i,s}, \text{ for all pixels } i\}. \quad (10)$$

Then, we estimate the camera intrinsic parameters,  $K$ , by applying the PerspectiveFields [29] model on image  $\mathcal{I}$ .

Last, we use the estimated correspondences,  $\mathcal{C}$ , and intrinsics  $K$ , to apply the RANSAC [20] and PnP [9] algorithms for estimating the object pose (or camera extrinsics). This pose, along with the initial object shape,  $\mathbf{z}_{init}$  (Sec. 3.3), initializes our fitting framework (Sec. 3.2).

## 4. Experiments

### 4.1. Implementation Details

Our SDFit framework fits a 3D mSDF to a single image.

**mSDF:** As mSDF (Sec. 3.1) we use the category-level DIT [75] model with pretrained weights for four categories (chair, sofa, car, airplane). In principle, SDFit would only get better as future mSDF models get better.

**Pose Init. (Sec. 3.4):** We establish image-to-shape correspondences by matching deep features. However, this is an unsolved task, so we sometimes falsely match left/right-side vertices and pixels, which is a known issue [73]. We tackle this via a simple-yet-effective heuristic. That is, we apply RANSAC+PnP on the established correspondences, and generate two hypotheses by mirroring pose around the vertical axis. Then, we refine each hypothesis over 200 iterations and select the one with the lower  $E_D$  from Eq. (2).

**Preprocessing:** Unlike competing methods, such as ZeroShape [27] and SDFusion [12], our SDFit does not require preprocessing. However, for a fair comparison, we follow ZeroShape by centering, padding, and downsampling images to a resolution of  $224 \times 224$ .

**Normal, Depth & Mask Maps:** For the objective function of Eq. (1) we need an observed ‘‘ground truth’’ segmentation mask,  $\mathcal{M}$ , normal map,  $\mathcal{N}$ , and depth map,  $\mathcal{D}$ , and respective maps rendered from the mSDF,  $\hat{\mathcal{M}}$ ,  $\hat{\mathcal{D}}$ , and  $\hat{\mathcal{N}}$ .

For  $\hat{\mathcal{M}}$ ,  $\hat{\mathcal{D}}$ ,  $\hat{\mathcal{N}}$ , we extract a mesh via FlexiCubes [60] with a grid size of  $N = 32$  and render with Nvdiffrast [35].

We estimate  $\mathcal{N}$  and  $\mathcal{D}$  by applying the OmniData [33] model on the input image. The masks  $\mathcal{M}$  can be provided by datasets (e.g., in Pix3D [62]), while in the opposite case (e.g., for Pascal3D+ [68]) we segment objects by applying the rembg [58] method (as in ZeroShape [27]).

**Fitting (Sec. 3.2):** We use the Adam optimizer [34]. For the first 300 iterations, we refine the initial pose,  $(R, t)$ , and scale,  $s$ , keeping shape  $S_{init}$  fixed. For the next 1000 iterations, we jointly optimize shape, scale and pose.

**Runtime:** We use an Nvidia 4080 GPU. Extracting image features [50, 74] takes 20 s, and decorating [18] a mesh 15 min for 100 views. Given features, fitting takes  $\sim 3min$ .

### 4.2. Metrics

We use three complementary numeric metrics as follows.

**Chamfer Distance (CD):** CD quantifies the similarity of two 3D point clouds  $X$  and  $Y$  as the average (bidirectional) distance from each point in a cloud to the nearest point in the other one. Then, with  $|\cdot|$  denoting cardinality,  $CD =$

$$\frac{1}{|X|} \sum_{x \in X} \min_{y \in Y} \|x - y\|_2 + \frac{1}{|Y|} \sum_{y \in Y} \min_{x \in X} \|x - y\|_2. \quad (11)$$

**F-Score:** Given a rejection threshold,  $d$ , the F-Score at distance  $d$  (FS@ $d$ ) is the harmonic mean of *precision@ $d$*  and *recall@ $d$* , reflecting the proportion of the surface accurately reconstructed within the correctness threshold  $d$ .

**Intersection-over-Union (IoU):** IoU encodes the alignment of an estimated 3D shape with image pixels, by quantifying the alignment between a target mask (detected in image) and estimated mask (projected 3D shape onto 2D) as:

$$IoU = \frac{TP}{TP + FP + FN} \times 100, \quad \text{where:} \quad (12)$$

TP is true positives, FP false positives, FN false negatives.

### 4.3. Tasks & Datasets

Our SDFit framework jointly recovers 3D object pose and shape. Therefore, we evaluate performance for two tasks, namely 3D shape (geometry) reconstruction and image alignment (involving both shape and pose reconstruction).

**Shape Reconstruction:** We evaluate the recovered 3D geometry alone, factoring out pose. We use the Pix3D [62] dataset that has real-world images paired with ground-truth CAD models. We use the test split of ZeroShape [27] for the *chair* and *sofa* categories. We evaluate our fitting-based SDFit method against the SotA data-driven SDFusion [12], ZeroShape [27], and OpenShape [38] methods.

	Pixel align.	Pix3D – Chair				Pix3D – Sofa			
		Mean CD ↓	FS@1 ↑	FS@2 ↑	FS@5 ↑	Mean CD ↓	FS@1 ↑	FS@2 ↑	FS@5 ↑
SDFusion [12]	✗	4.79	0.12	0.29	0.63	N/A	N/A	N/A	N/A
OpenShape [38]	✗	4.53	0.12	0.32	0.65	3.53	0.21	0.46	0.81
ZeroShape [27]	~	4.54	0.15	0.33	0.66	<b>2.34</b>	0.30	<b>0.60</b>	<b>0.89</b>
SDFit (Ours) $feat@T$	✓	4.12	0.17	0.37	0.71	3.23	0.24	0.52	0.79
SDFit (Ours) $feat@S_{init}$	✓	<b>4.03</b>	<b>0.17</b>	<b>0.38</b>	<b>0.72</b>	3.03	<b>0.32</b>	0.53	0.82

Table 1. Shape reconstruction performance on Pix3D [62] chair and sofa categories. The column “pixel alignment” indicates whether a method infers both object shape and object/camera pose, so that the reconstructed 3D object can be aligned with the input image (i.e., whether it can be rendered as an overlay on top of the image). Bold numbers indicate the best performer per column. Metrics include the mean Chamfer Distance and F-Score at three different thresholds. Arrows indicate whether a higher or lower value is desired per metric.

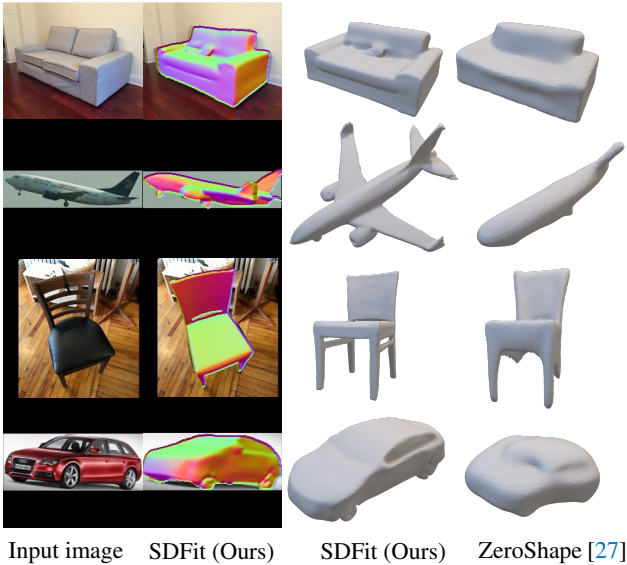


Figure 6. Evaluation of shape recovery for SDFit ( $feat@S_{init}$ ) and ZeroShape [27]. SDFit jointly fits pose and shape to the image, facilitating pixel alignment. It also excels at recovering occluded parts through the mSDF’s learned shape prior. For overlays we show the mSDF’s normals for technical visualization reasons.

We summarize results in Tab. 1, where we report the Chamfer Distance (CD) and F-Score. Our SDFit outperforms competition for the chair category across all metrics. For the sofa category the competing ZeroShape performs better. This can be attributed on two unsolved problems, i.e., estimating from an image accurate: (1) camera intrinsics,  $K$ , and (2) depth and normal maps,  $\mathcal{D}$  and  $\mathcal{N}$ . That is, SDFit sometimes infers reasonable but elongated sofa shapes, which, project onto the right pixels during render-and-compare fitting due to errors in above estimates.

We qualitatively compare the best performers of Tab. 1, namely SDFit and ZeroShape [27], in Fig. 6. ZeroShape struggles recovering self-occluded object parts. Instead, our SDFit recovers these via the mSDF’s learned shape prior. Note that ZeroShape performs feed-forward inference, so it cannot correct false predictions. Instead, SDFit refines estimates in an iterative render-and-compare fashion.

Note that ZeroShape takes masked images as input, i.e., scene context is ignored, and infers proxy depth maps and camera intrinsics from these, for later recovering visible object points. Thus, shape prediction depends highly on proxy estimates that are sometimes noisy. Instead, we estimate intrinsics by applying PerspectiveFields [29] on the full image that includes scene context, so it infers empirically more robust intrinsics. Moreover, even though SDFit also uses proxy normal and depth maps,  $\mathcal{N}$  and  $\mathcal{D}$ , it further exploits deep foundational features and correspondences for recovering visible points and initializing pose, respectively, which makes it more robust to noisy proxy estimates.

**Image Alignment:** We evaluate joint shape-and-pose estimation that ideally recovers image-aligned 3D objects. We use the real-world Pascal3D+ [68] dataset and specifically the test split of Pavlo et al. [54] that includes the car and airplane categories. Since SotA 3D reconstruction methods focus mostly on shape recovery, often ignoring pose, we establish our own two-step baselines as follows: (1) We first infer (canonical-scale) shape through SotA regression [27], diffusion [12], and retrieval [7] methods. (2) We then keep shape fixed, and optimize over pose and scale in a render-and-compare (RnC) fashion as in Eq. (1). For fairness, for all methods we initialize the camera extrinsics and intrinsics using our SDFit’s steps (Sec. 3.4), with the only exception being ZeroShape that inherently considers the world and camera frames to be aligned, so, we only need to initialize the extrinsic translation.

Table 2 reports results via the Intersection-over-Union metric. SDFit  $feat@S_{init}$  outperforms baselines, while SDFit  $feat@T$  is on par with ZeroShape + RnC but outperforms others. All baselines start with a similar pose initialization. Thus, SDFit’s better performance is partially due to its joint pose and shape fitting. That is, SDFit refines not only the initial pose, but also the shape by morphing the mSDF. Note that ZeroShape infers shape in camera frame, implicitly considering image alignment, so it performs better than other baselines, though worse than SDFit.

We conclude that SDFit’s joint fitting is crucial for pixel alignment, as pose and shape are inherently interdependent. Note that SDFit, uniquely, needs no retraining in the wild.

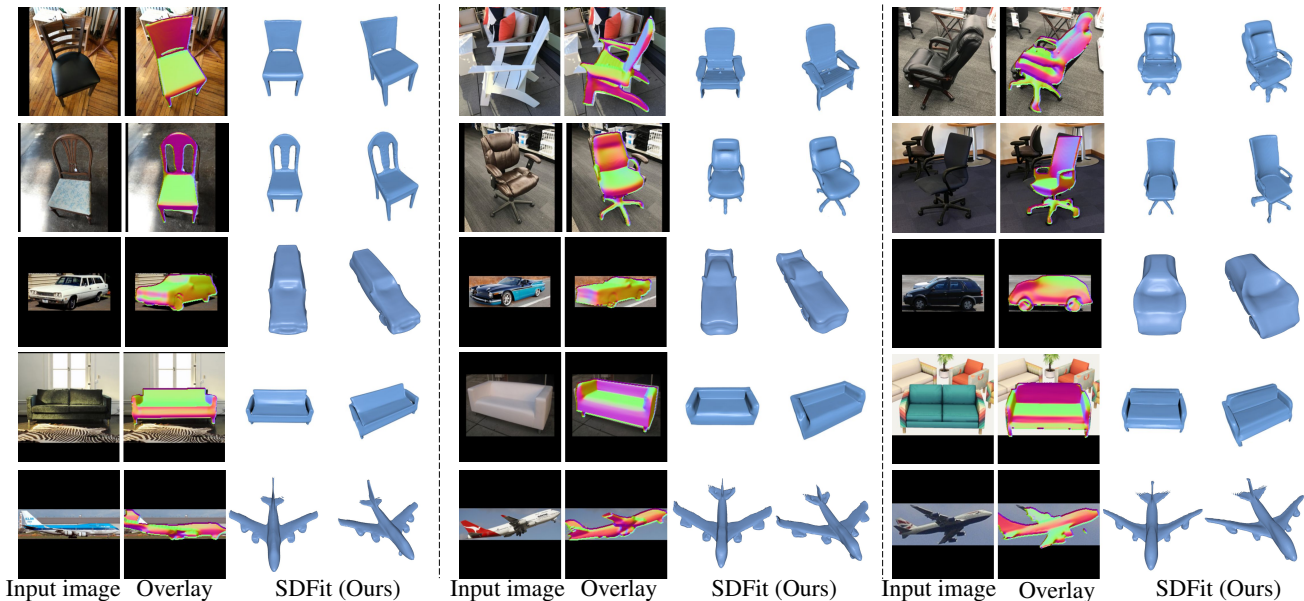


Figure 7. Qualitative results for SDFit ( $\text{feat}@S_{init}$ ) on Pix3D [62] and Pascal3D+ [68] images. We show the estimated 3D shape (left to right) in camera- (as normal map), front- and side-view, for four classes, i.e., chair, car, sofa, airplane. **Q Zoom in** to see details.

Metric: IoU (%) $\uparrow$	Pascal3D+		Pix3D		Mean IoU
	Plane	Car	Chair	Sofa	
SDFusion [12] + RnC	N/A	N/A	59.5	N/A	N/A
OpenShape [38] + RnC	48.5	79.5	54.3	85.2	66.8
ZeroShape [27] + RnC	76.4	89.1	61.3	85.9	78.1
SDFit (Ours) $\text{feat}@T$	77.6	86.9	61.1	89.7	78.8
SDFit (Ours) $\text{feat}@S_{init}$	<b>81.5</b>	<b>91.6</b>	<b>75.9</b>	<b>92.7</b>	<b>85.4</b>

Table 2. Image-alignment performance on the Pascal3D+ [68] and Pix3D [62] datasets. The shape predictions of competing methods are aligned to the image in a render-and-compare (RnC) fashion similarly to our SDFit. We report the per-category IoU metric, as well as the Mean IoU across all categories.

Note that Tab. 1 and Tab. 2 report two SDFit versions, namely “SDFit  $\text{feat}@T$ ” and “SDFit  $\text{feat}@S_{init}$ ”. The correspond to the two pose initialization methods discussed in Sec. 3.4 and Fig. 5. These options trade efficiency for accuracy; the former is computationally cheaper, but the latter is more accurate because the topology of  $S_{init}$  agrees with the image more often than  $T$ .

**Qualitative Results:** We show extensive qualitative results of our SDFit ( $\text{feat}@S_{init}$ ) for in-the-wild Pix3D [62] and Pascal3D+ [68] images in Fig. 7. We see that SDFit effectively reconstructs 3D shapes that are not only visually consistent with the input images, but also pixel aligned. Note that in-the-wild images have a huge diversity for objects and imaging conditions, which significantly challenges purely data-driven methods. Instead, SDFit shows a unique and promising generalization capability to real-world data, even in challenging scenarios with significant perspective distortion. Moreover, unlike purely data-driven methods, SDFit doesn’t need retraining to this end.

## 5. Conclusion

We recover 3D object pose and shape from single images, a challenging task due to self-occlusions, depth ambiguities, highly varying shapes, and lack of annotated images. Specifically, we develop a novel framework, called SDFit, that exploits a category-level 3D morphable SDF model for generating shape hypotheses, and fitting this to image cues in a render-and-compare fashion. To this end, SDFit exploits recent foundational models for initializing shape via a retrieval-based method, extracting 2D-to-3D image-to-shape correspondences for initializing pose, and estimating robust normal and depth maps for render-and-compare. SDFit performs on par with SotA data-driven methods on real-world datasets Pix3D [62] and Pascal3D+ [68], but, uniquely, requires no re-training in the wild. Thus, SDFit is promising and opens up ways for future research.

**Future Work:** We build on DIT [75], consequently, we are limited to DIT’s latent space and four object classes. Future work will learn a more flexible latent space and expand it to more classes using large CAD databases [8, 15, 66]. In tandem with such databases, we believe the future might lie in 3D object data crowd-sourced from mixed-reality headsets [3, 47, 48]. Moreover, addressing left-right ambiguities in visual features [73] would help correspondence matching, while more involved heuristics for choosing over multiple initial pose hypotheses could help. Last, we will explore initializing SDFit with a learned regression component [36].

**Acknowledgements:** We thank Božidar Antić, Yuliang Xiu and Muhammed Kocabas for helpful insights. D. Tzionas is supported by the ERC Starting Grant (project STRIPES, 101165317).

**Disclosure:** D. Tzionas has received a research gift from Google.



## References

- [1] Kalyan Vasudev Alwala, Abhinav Gupta, and Shubham Tulsiani. Pretrain, self-train, distill: A simple recipe for super-sizing 3D reconstruction. In *CVPR*, pages 3763–3772, 2022. 2, 3
- [2] Dragomir Anguelov, Praveen Srinivasan, Daphne Koller, Sebastian Thrun, Jim Rodgers, and James Davis. SCAPE: Shape completion and animation of people. *TOG*, 24:408–416, 2005. 2
- [3] Apple Vision Pro. Mixed-reality headset. <https://www.apple.com/apple-vision-pro>, 2024. 8
- [4] Muhammad Awais, Muzammal Naseer, Salman Khan, Rao Muhammad Anwer, Hisham Cholakkal, Mubarak Shah, Ming-Hsuan Yang, and Fahad Shahbaz Khan. Foundational models defining a new era in vision: A survey and outlook. arXiv:2307.13721, 2023. 3
- [5] Mohamed El Banani, Amit Raj, Kevis-Kokitsi Maninis, Abhishek Kar, Yuanzhen Li, Michael Rubinstein, Deqing Sun, Leonidas Guibas, Justin Johnson, and Varun Jampani. Probing the 3D awareness of visual foundation models. In *CVPR*, pages 21795–21806, 2024. 3, 5
- [6] Federica Bogo, Angjoo Kanazawa, Christoph Lassner, Peter Gehler, Javier Romero, and Michael J. Black. Keep it SMPL: Automatic estimation of 3D human pose and shape from a single image. In *ECCV*, pages 561–578, 2016. 2
- [7] Zhe Cao, Gines Hidalgo, Tomas Simon, Shih-En Wei, and Yaser Sheikh. OpenPose: Realtime multi-person 2D pose estimation using part affinity fields. *TPAMI*, 43(1):172–186, 2021. 2, 7
- [8] Angel X. Chang, Thomas Funkhouser, Leonidas Guibas, Pat Hanrahan, Qixing Huang, Zimo Li, Silvio Savarese, Manolis Savva, Shuran Song, Hao Su, Jianxiang Xiao, Li Yi, and Fisher Yu. ShapeNet: An information-rich 3D model repository. arXiv:1512.03012, 2015. 2, 3, 4, 8
- [9] Bo Chen, Álvaro Parra, Jiewei Cao, Nan Li, and Tat-Jun Chin. End-to-end learnable geometric vision by backpropagating PnP optimization. In *CVPR*, pages 8097–8106, 2019. 3, 6
- [10] Hansheng Chen, Yuyao Huang, Wei Tian, Zhong Gao, and Lu Xiong. MonoRUn: Monocular 3D object detection by reconstruction and uncertainty propagation. In *CVPR*, pages 10379–10388, 2021. 3
- [11] Zhiqin Chen and Hao Zhang. Learning implicit fields for generative shape modeling. In *CVPR*, pages 5939–5948, 2019. 3
- [12] Yen-Chi Cheng, Hsin-Ying Lee, Sergey Tuyakov, Alex Schwing, and Liangyan Gui. SDFusion: Multimodal 3D shape completion, reconstruction, and generation. In *CVPR*, pages 4456–4465, 2023. 2, 3, 6, 7, 8
- [13] Vasileios Choutas, Georgios Pavlakos, Timo Bolkart, Dimitrios Tzionas, and Michael J. Black. Monocular expressive body regression through Body-Driven attention. In *ECCV*, pages 20–40, 2020. 2
- [14] Christopher B. Choy, Danfei Xu, JunYoung Gwak, Kevin Chen, and Silvio Savarese. 3D-R2N2: A unified approach for single and multi-view 3D object reconstruction. *ECCV*, 9912:628–644, 2016. 3
- [15] Matt Deitke, Ruoshi Liu, Matthew Wallingford, Huong Ngo, Oscar Michel, Aditya Kusupati, Alan Fan, Christian Laforte, Vikram Voleti, Samir Yitzhak Gadre, Eli VanderBilt, Aniruddha Kembhavi, Carl Vondrick, Georgia Gkioxari, Kiana Ehsani, Ludwig Schmidt, and Ali Farhadi. Objaverse-XL: A universe of 10M+ 3D objects. In *NeurIPS*, 2023. 2, 8
- [16] Matt Deitke, Dustin Schwenk, Jordi Salvador, Luca Weihs, Oscar Michel, Eli VanderBilt, Ludwig Schmidt, Kiana Ehsani, Aniruddha Kembhavi, and Ali Farhadi. Objaverse: A universe of annotated 3D objects. In *CVPR*, pages 13142–13153, 2023. 2
- [17] Congyue Deng, Chiyu Max Jiang, Charles R. Qi, Xinchen Yan, Yin Zhou, Leonidas J. Guibas, and Dragomir Anguelov. NeRDi: Single-view NeRF synthesis with Language-Guided diffusion as general image priors. In *CVPR*, pages 20637–20647, 2023. 2
- [18] Niladri Shekhar Dutt, Sanjeev Muralikrishnan, and Niloy J. Mitra. Diffusion 3D features (Diff3F): Decorating untextured shapes with distilled semantic features. arXiv:2311.17024, 2023. 5, 6
- [19] Haoqiang Fan, Hao Su, and Leonidas Guibas. A point set generation network for 3D object reconstruction from a single image. *CVPR*, pages 2463–2471, 2017. 3
- [20] Martin A. Fischler and Robert C. Bolles. Random sample consensus: A paradigm for model fitting with applications to image analysis and automated cartography. *Communications of the ACM*, 24(6):381–395, 1981. 6
- [21] Georgia Gkioxari, Jitendra Malik, and Justin Johnson. Mesh R-CNN. *ICCV*, pages 9784–9794, 2019. 3
- [22] Walter Goodwin, Sagar Vaze, Ioannis Havoutis, and Ingmar Posner. Zero-shot category-level object pose estimation. In *ECCV*, pages 516–532, 2022. 3
- [23] Can Gümeli, Angela Dai, and Matthias Nießner. ROCA: Robust CAD model retrieval and alignment from a single image. In *CVPR*, pages 4012–4021, 2022. 3
- [24] Ziyu Guo, Renrui Zhang, Xiangyang Zhu, Yiwen Tang, Xi-anzheng Ma, Jiaming Han, Kexin Chen, Peng Gao, Xi-anzhi Li, Hongsheng Li, and Pheng-Ann Heng. Point-Bind & Point-LLM: Aligning point cloud with multi-modality for 3D understanding, generation, and instruction following. arXiv:2309.00615, 2023. 2
- [25] Yicong Hong, Kai Zhang, Jiuxiang Gu, Sai Bi, Yang Zhou, Difan Liu, Feng Liu, Kalyan Sunkavalli, Trung Bui, and Hao Tan. LRM: Large reconstruction model for single image to 3D. In *ICLR*, 2024. 2, 3
- [26] Zixuan Huang, Varun Jampani, Anh Thai, Yuanzhen Li, Stefan Stojanov, and James M. Rehg. ShapeClipper: Scalable 3D shape learning from single-view images via geometric and CLIP-based consistency. In *CVPR*, pages 12912–12922, 2023. 3
- [27] Zixuan Huang, Stefan Stojanov, Anh Thai, Varun Jampani, and James M. Rehg. ZeroShape: Regression-based zero-shot shape reconstruction. In *CVPR*, pages 10061–10071, 2024. 2, 3, 6, 7, 8
- [28] Won Jun Jang and Lourdes de Agapito. CodeNeRF: Disentangled neural radiance fields for object categories. *ICCV*, pages 12929–12938, 2021. 3

- [29] Linyi Jin, Jianming Zhang, Yannick Hold-Geoffroy, Oliver Wang, Kevin Matzen, Matthew Sticha, and David F. Fouhey. Perspective fields for single image camera calibration. In *CVPR*, pages 17307–17316, 2023. 6, 7
- [30] Hanbyul Joo, Tomas Simon, and Yaser Sheikh. Total capture: A 3D deformation model for tracking faces, hands, and bodies. In *CVPR*, pages 8320–8329, 2018. 2
- [31] Hanbyul Joo, Natalia Neverova, and Andrea Vedaldi. Exemplar fine-tuning for 3D human pose fitting towards in-the-wild 3D human pose estimation. In *3DV*, pages 42–52, 2021. 2
- [32] Heewoo Jun and Alex Nichol. Shap-E: Generating conditional 3D implicit functions. arXiv:2305.02463, 2023. 2, 3
- [33] Oğuzhan Fatih Kar, Teresa Yeo, Andrei Atanov, and Amir Zamir. 3D common corruptions and data augmentation. In *CVPR*, pages 18963–18974, 2022. 6
- [34] Diederik P. Kingma and Jimmy Ba. Adam: A method for stochastic optimization. In *ICLR*, 2015. 6
- [35] Samuli Laine, Janne Hellsten, Tero Karras, Yeongho Seol, Jaakko Lehtinen, and Timo Aila. Modular primitives for high-performance differentiable rendering. *TOG*, 39(6), 2020. 6
- [36] Kailin Li, Lixin Yang, Haoyu Zhen, Zenan Lin, Xinyu Zhan, Licheng Zhong, Jian Xu, Kejian Wu, and Cewu Lu. CHORD: Category-level hand-held object reconstruction via shape deformation. In *ICCV*, pages 9410–9420, 2023. 8
- [37] Zhihao Li, Jianzhuang Liu, Zhensong Zhang, Songcen Xu, and Youliang Yan. CLIFF: carrying location information in full frames into human pose and shape estimation. In *ECCV*, pages 590–606, 2022. 2
- [38] Minghua Liu, Ruoxi Shi, Kaiming Kuang, Yinhao Zhu, Xuanlin Li, Shizhong Han, Hong Cai, Fatih Porikli, and Hao Su. OpenShape: Scaling up 3D shape representation towards open-world understanding. In *NeurIPS*, 2023. 2, 3, 4, 5, 6, 7, 8
- [39] Minghua Liu, Chao Xu, Haiyan Jin, Linghao Chen, Mukund Varma T, Zexiang Xu, and Hao Su. One-2-3-45: Any single image to 3D mesh in 45 seconds without per-shape optimization. *NeurIPS*, 2024. 3
- [40] Ruoshi Liu, Rundi Wu, Basile Van Hoorick, P. Tokmakov, Sergey Zakharov, and Carl Vondrick. Zero-1-to-3: Zero-shot one image to 3D object. *ICCV*, pages 9264–9275, 2023. 3
- [41] Zongdai Liu, Dingfu Zhou, Feixiang Lu, Jin Fang, and Liangjun Zhang. AutoShape: Real-time shape-aware monocular 3D object detection. In *ICCV*, pages 15621–15630, 2021. 3
- [42] Matthew Loper, Naureen Mahmood, Javier Romero, Gerard Pons-Moll, and Michael J. Black. SMPL: A skinned multi-person linear model. *TOG*, 34(6):248:1–248:16, 2015. 2
- [43] Camillo Lugaresi, Jiuqiang Tang, Hadon Nash, Chris McClanahan, Esha Uboweja, Michael Hays, Fan Zhang, Chuoling Chang, Ming Guang Yong, Juhyun Lee, Wan-Teh Chang, Wei Hua, Manfred Georg, and Matthias Grundmann. MediaPipe: A framework for building perception pipelines. In *CVPRW*, 2019. 2
- [44] Grace Luo, Lisa Dunlap, Dong Huk Park, Aleksander Holynski, and Trevor Darrell. Diffusion hyperfeatures: Searching through time and space for semantic correspondence. In *NeurIPS*, 2023. 5
- [45] Luke Melas-Kyriazi, Iro Laina, Christian Rupprecht, and Andrea Vedaldi. Realfusion 360° reconstruction of any object from a single image. In *CVPR*, pages 8446–8455, 2023. 2, 3
- [46] Luke Melas-Kyriazi, Christian Rupprecht, and Andrea Vedaldi. PC<sup>2</sup>: Projection-conditioned point cloud diffusion for single-image 3D reconstruction. In *CVPR*, pages 12923–12932, 2023. 2
- [47] Meta Quest. Mixed-reality headset. <https://www.meta.com/nl/en/quest>, 2024. 8
- [48] Microsoft HoloLens. Mixed-reality headset. <https://www.microsoft.com/en-us/hololens>, 2024. 8
- [49] Alex Nichol, Heewoo Jun, Prafulla Dhariwal, Pamela Mishkin, and Mark Chen. Point-E: A system for generating 3D point clouds from complex prompts. arXiv:2212.08751, 2022. 2, 3
- [50] Maxime Oquab, Timothée Darcet, Théo Moutakanni, Huy Vo, Marc Szafraniec, Vasil Khalidov, Pierre Fernandez, Daniel Haziza, Francisco Massa, Alaaeldin El-Nouby, Mahmoud Assran, Nicolas Ballas, Wojciech Galuba, Russell Howes, Po-Yao Huang, Shang-Wen Li, Ishan Misra, Michael Rabbat, Vasu Sharma, Gabriel Synnaeve, Hu Xu, Hervé Jegou, Julien Mairal, Patrick Labatut, Armand Joulin, and Piotr Bojanowski. DINOv2: Learning robust visual features without supervision. *TMLR*, 2024. 2, 3, 4, 5, 6
- [51] Evin Pinar Örnek, Yann Labbé, Bugra Tekin, Lingni Ma, Cem Keskin, Christian Forster, and Tomas Hodan. FoundPose: Unseen object pose estimation with foundation features. In *ECCV*, 2024. 3
- [52] Jeong Joon Park, Peter R. Florence, Julian Straub, Richard A. Newcombe, and Steven Lovegrove. DeepSDF: Learning continuous signed distance functions for shape representation. In *CVPR*, pages 165–174, 2019. 2, 3
- [53] Georgios Pavlakos, Vasileios Choutas, Nima Ghorbani, Timo Bolkart, Ahmed A. A. Osman, Dimitrios Tzionas, and Michael J. Black. Expressive body capture: 3D hands, face, and body from a single image. In *CVPR*, pages 10975–10985, 2019. 2
- [54] Dario Pavllo, Jonas Kohler, Thomas Hofmann, and Aurelien Lucchi. Learning generative models of textured 3D meshes from real-world images. In *ICCV*, pages 13859–13869, 2021. 7
- [55] Dario Pavllo, David Joseph Tan, Marie-Julie Rakotosaona, and Federico Tombari. Shape, pose, and appearance from a single image via bootstrapped radiance field inversion. In *CVPR*, pages 4391–4401, 2023. 3
- [56] Guocheng Qian, Jinjie Mai, Abdullah Hamdi, Jian Ren, Aliaksandr Siarohin, Bing Li, Hsin-Ying Lee, Ivan Skokhodov, Peter Wonka, Sergey Tulyakov, and Bernard Ghanem. Magic123: One image to high-quality 3D object generation using both 2D and 3D diffusion priors. In *ICLR*, 2024. 3
- [57] René Ranftl, Katrin Lasinger, David Hafner, Konrad Schindler, and Vladlen Koltun. Towards robust monocular

- depth estimation: Mixing datasets for zero-shot cross-dataset transfer. *TPAMI*, 44(3):1623–1637, 2022. 4
- [58] Rembg: A tool to remove images background. <https://github.com/danielgatis/rembg>, 2022. 6
- [59] Robin Rombach, Andreas Blattmann, Dominik Lorenz, Patrick Esser, and Björn Ommer. High-resolution image synthesis with latent diffusion models. In *CVPR*, pages 10674–10685, 2022. 2, 3, 5
- [60] Tianchang Shen, Jacob Munkberg, Jon Hasselgren, Kangxue Yin, Zian Wang, Wenzheng Chen, Zan Gojcic, Sanja Fidler, Nicholas Sharp, and Jun Gao. Flexible isosurface extraction for gradient-based mesh optimization. *TOG*, 42(4):37:1–37:16, 2023. 4, 6
- [61] Vincent Sitzmann, Julien N. P. Martel, Alexander W. Bergman, David B. Lindell, and Gordon Wetzstein. Implicit neural representations with periodic activation functions. In *NeurIPS*, 2020. 2
- [62] Xingyuan Sun, Jiajun Wu, Xiuming Zhang, Zhoutong Zhang, Chengkai Zhang, Tianfan Xue, Joshua B Tenenbaum, and William T Freeman. Pix3D: Dataset and methods for single-image 3D shape modeling. In *CVPR*, pages 2974–2983, 2018. 2, 6, 7, 8
- [63] He Wang, Srinath Sridhar, Jingwei Huang, Julien P. C. Valentin, Shuran Song, and L. Guibas. Normalized object coordinate space for category-level 6D object pose and size estimation. In *CVPR*, pages 2642–2651, 2019. 3
- [64] Nanyang Wang, Yinda Zhang, Zhuwen Li, Yanwei Fu, W. Liu, and Yu-Gang Jiang. Pixel2Mesh: Generating 3D mesh models from single RGB images. In *ECCV*, pages 55–71, 2018. 3
- [65] Rundi Wu, Yixin Zhuang, Kai Xu, Hao Zhang, and Baoquan Chen. PQ-NET: A generative part Seq2Seq network for 3D shapes. *CVPR*, pages 826–835, 2020. 3
- [66] Tong Wu, Jiarui Zhang, Xiao Fu, Yuxin Wang, Jiawei Ren, Liang Pan, Wayne Wu, Lei Yang, Jiaqi Wang, Chen Qian, Dahua Lin, and Ziwei Liu. OmniObject3D: Large-Vocabulary 3D object dataset for realistic perception, reconstruction and generation. In *CVPR*, pages 803–814, 2023. 2, 8
- [67] Donglai Xiang, Hanbyul Joo, and Yaser Sheikh. Monocular total capture: Posing face, body, and hands in the wild. In *CVPR*, pages 10957–10966, 2019. 2
- [68] Yu Xiang, Roozbeh Mottaghi, and Silvio Savarese. Beyond PASCAL: A benchmark for 3D object detection in the wild. In *WACV*, pages 75–82, 2014. 2, 6, 7, 8
- [69] Yu Xiang, Tanner Schmidt, Venkatraman Narayanan, and Dieter Fox. PoseCNN: A convolutional neural network for 6D object pose estimation in cluttered scenes. *Robotics: Science and Systems (RSS)*, 2018. 3
- [70] Hongyi Xu, Eduard Gabriel Bazavan, Andrei Zanfir, William T. Freeman, Rahul Sukthankar, and Cristian Sminchisescu. GHUM & GHUML: Generative 3D human shape and articulated pose models. In *CVPR*, pages 6183–6192, 2020. 2
- [71] Yufei Ye, Shubham Tulsiani, and Abhinav Gupta. Shelf-supervised mesh prediction in the wild. In *CVPR*, pages 8843–8852, 2021. 3
- [72] Junyi Zhang, Charles Herrmann, Junhwa Hur, Luisa Polania Cabrera, Varun Jampani, Deqing Sun, and Ming-Hsuan Yang. A tale of two features: Stable diffusion complements DINO for zero-shot semantic correspondence. In *NeurIPS*, 2023. 2, 5
- [73] Junyi Zhang, Charles Herrmann, Junhwa Hur, Eric Chen, Varun Jampani, Deqing Sun, and Ming-Hsuan Yang. Telling left from right: Identifying geometry-aware semantic correspondence. In *CVPR*, pages 3076–3085, 2024. 6, 8
- [74] Lvmin Zhang, Anyi Rao, and Maneesh Agrawala. Adding conditional control to Text-to-Image diffusion models. In *ICCV*, pages 3836–3847, 2023. 2, 3, 4, 5, 6
- [75] Zerong Zheng, Tao Yu, Qionghai Dai, and Yebin Liu. Deep implicit templates for 3D shape representation. In *CVPR*, pages 1429–1439, 2021. 1, 2, 3, 4, 5, 6, 8
- [76] Junsheng Zhou, Jinsheng Wang, Baorui Ma, Yu-Shen Liu, Tiejun Huang, and Xinlong Wang. Uni3D: Exploring unified 3D representation at scale. In *ICLR*, 2024. 2, 3